PROCEEDINGS OF SCIENCE

Baryon-baryon Interactions from Lattice QCD

Noriyoshi Ishii for HAL QCD Collaboration*
Kobe-branch, Center for Computational Sciences, University of Tsukuba
E-mail: ishii@ribf.riken.jp

Lattice QCD study of baryon-baryon interaction is reported. We use equal-time Nambu-Bethe-Salpeter (NBS) wave functions to define baryon-baryon potentials by Schrödinger equation. Resultant potentials are faithful to scattering data, because they are defined to reproduce the scattering phase which is embedded in equal-time NBS wave functions at long spatial region. The potentials thus defined are more efficiently obtained from four-point baryon correlators, which enables us to construct the potentials without relying on the ground state saturation. These techniques are used to study various systems such as two-nucleon system, three-nucleon system and two-hyperon systems.

The 7th International Workshop on Chiral Dynamics,
August 6 -10, 2012
Jefferson Lab, Newport News, Virginia, USA

*Speaker.

PoS(CD12)025

1. Introduction

Scattering phase is an important physical observable. However, it is more advantageous to convert it into a form of the nuclear potential (nuclear force). Once such a nuclear potential is constructed, it is conveniently used to study a variety of phenomena in multi-nucleon system. It provides us with physics insights into structures and reactions of atomic nuclei based on the nucleon, the relevant effective degrees of freedom at low energy. It has an important influence on the astrophysics such as the supernova explosion of type II and the structure of neutron stars through the equation of states of cold and dense nuclear matter. Enormous efforts have been devoted to the construction of realistic nuclear potentials [1, 2, 3]. By using about $40-50$ adjustable parameters, these realistic nuclear potentials can reproduce several thousands of experimental NN data with $\chi^2/\mathrm{NDF} \sim 1$, which consist of the scattering phase and the deuteron property. Recently, the nuclear potentials based on the chiral effective field theory has been developed, which attracts an growing interest in nuclear physics [4].

Unlike the ordinary two-nucleon sector, number of experimental information is too small to construct realistic potentials in the hyperon sector. This is due to the short life time of hyperons, which makes it difficult to perform direct scattering experiments. If realistic hyperon potentials would exist, it could help us understand the structure of hyper-nuclei and possible generation of hyperon matter in the neutron star core. The situation is similar for the three-nucleon potential, which is expected to provide an important contribution at high density.

For those systems where experimental input is limited, we desire to have an alternative method. A strong candidate would be the lattice QCD Monte Carlo calculation. Recently, a lattice QCD method to determine hadron potentials has been developed by HAL QCD collaboration [5, 6, 7, 8, 9, 10, 11]. It has been extensively applied to many systems [12, 13, 14, 15, 16, 17, 18, 19, 20, 21, 22]. With this method, potentials are constructed from equal-time Nambu-Bethe-Salpeter (NBS) wave functions. Because the information of scattering phase is embedded in the long distance behaviors of NBS wave function, the resultant potentials are faithful to scattering data.

In this paper, after a brief review of the general idea how to define and construct a realistic nuclear potential in lattice QCD, we present our recent progress on the NN potentials, three-nucleon potential, and hyperon potentials.

2. General idea

2.1 Definition of the potential

To define the nuclear potential, we consider Nambu-Bethe-Salpeter (NBS) wave function for two-nucleon system in the center of mass (CM) frame. To simplify the notation, we treat a nucleon as a scalar boson in this section. (Extension to Dirac fermions is straightforward.) By choosing a particular composite interpolating fields $N(x)$ for a baryon, NBS wave function is written as

$$\psi_{\vec{k}}(x-y) \equiv Z_N^{-1} \left\langle 0 \left| T[N(x)N(y)] \right| N(\vec{k})N(-\vec{k}), \mathrm{in} \right\rangle, \tag{2.1}$$

where $\vec{k}$ denotes the asymptotic momentum. It is related to the relativistic total energy by $E_{\mathrm{CM}} = 2\sqrt{m_N^2 + \vec{k}^2}$ with m_N being the baryon mass. Z_N denotes the normalization factor involved in the limit $N(x) \to Z_N^{1/2} N_{\mathrm{out}}(x)$ as $x_0 \to +\infty$.

NBS wave function is related to the S-matrix through the reduction formula

$$\begin{aligned}&\langle N(\vec{p})N(-\vec{p}),\text{out}|N(\vec{k})N(-\vec{k}),\text{in}\rangle \\ &= \text{disc.} + i^2 \int d^4x_1\, d^4x_2\, e^{ip_1x_1}(\Box_1 + m_N^2)\, e^{ip_2x_2}(\Box_2 + m_N^2)\, \psi_{\vec{k}}(x_1,x_2).\end{aligned} \tag{2.2}$$

This formula can be used to derive the asymptotic form of the equal-time restriction of NBS wave function at long spatial distance, i.e., $|\vec{x}-\vec{y}| \to$ large [6, 23, 24]

$$\psi_{\vec{k}}(\vec{x}-\vec{y}) \equiv \lim_{x_0\to+0} \psi_{\vec{k}}(\vec{x},x_0;\vec{y},y_0=0) \simeq e^{i\delta_0(k)} \frac{\sin(kr+\delta_0(k))}{kr} + \cdots, \text{ (s-wave)} \tag{2.3}$$

where $\delta_0(k)$ denotes the scattering phase. It is important to note that it has the same functional form as the scattering wave function in the quantum mechanics. In Lüscher's finite volume method, which is the standard method to calculate the scattering phase in lattice QCD, the scattering phase in NBS wave function is extracted from the energy spectrum in a finite periodic box [25]. (For an explicit use of equal-time NBS wave function in Lüscher's method, see Ref. [24].)

To define the nuclear potential, we use the fact that equal-time NBS wave function has the same asymptotic form as scattering wave function of non-relativistic quantum mechanics. We introduce our nuclear potentials by demanding that Schrödinger equation should reproduce the equal-time NBS wave functions in the energy region below the pion threshold, i.e., $E_{\text{CM}} \lesssim E_{\text{th}} \equiv 2m_N + m_\pi$ as

$$(\vec{k}^2/m_N - H_0)\psi_{\vec{k}}(\vec{r}) = \int d^3r'\, U(\vec{r},\vec{r}')\psi_{\vec{k}}(\vec{r}'), \tag{2.4}$$

where $H_0 \equiv -\vec{\nabla}^2/m_N$ denotes the unperturbed Hamiltonian for two-nucleon system in the CM frame. Note that the resultant potential $U(\vec{r},\vec{r}')$ is faithful to the scattering phase, because equal-time NBS wave functions contain the scattering phase in their long distance part as Eq. (2.3)

The potential $U(\vec{r},\vec{r}')$ so defined becomes a non-local operator in general. But, it can be define to be independent of energy E.[1] To see this, we first assume that $\psi_{\vec{k}}(\vec{r})$ for different $\vec{k}$ is linearly independent from each other. Then, $\psi_{\vec{k}}(\vec{r})$ has a dual basis $\tilde{\psi}_{\vec{k}}(\vec{r})$, which serves as a "left inverse" as

$$\int d^3r\, \tilde{\psi}_{\vec{k}'}(\vec{r})\psi_{\vec{k}}(\vec{r}) = (2\pi)^3\delta^3(\vec{k}'-\vec{k}). \tag{2.5}$$

By using this, we have

$$\begin{aligned}K_{\vec{k}}(\vec{r}) &\equiv \left(\vec{k}^2/m_N - H_0\right)\psi_{\vec{k}}(\vec{r}) \\ &= \int \frac{d^3k'}{(2\pi)^3} K_{\vec{k}'}(\vec{r}) \int d^3r'\, \tilde{\psi}_{\vec{k}'}(\vec{r}')\psi_{\vec{k}}(\vec{r}') = \int d^3r' \left[\int \frac{d^3k'}{(2\pi)^3} K_{\vec{k}'}(\vec{r})\tilde{\psi}_{\vec{k}'}(\vec{r}')\right]\psi_{\vec{k}}(\vec{r}').\end{aligned} \tag{2.6}$$

Eq. (2.4) is arrived at, if we define $U(\vec{r},\vec{r}')$ as

$$U(\vec{r},\vec{r}') \equiv \int \frac{d^3k}{(2\pi)^3} K_{\vec{k}}(\vec{r})\tilde{\psi}_{\vec{k}}(\vec{r}'). \tag{2.7}$$

We see that, due to the integration over $\vec{k}$, $U(\vec{r},\vec{r}')$ depend neither on $\vec{k}$ nor on the energy $E \equiv \vec{k}^2/m_N$.

[1] Our definition is different from the one given in Ref. [25], where an effective Schrödinger equation with energy-dependent potential is defined.

Non-local potentials are not convenient in practice. We therefore apply the derivative expansion to express $U(\vec{r},\vec{r}')$ as a series of products of local functions and differential operators as $U(\vec{r},\vec{r}') = V(\vec{r},\vec{\nabla})\delta(\vec{r}-\vec{r}')$ with

$$V(\vec{r},\vec{\nabla}) = V_0(r) + V_\sigma(r)\vec{\sigma}_1\cdot\vec{\sigma}_2 + V_{\rm T}(r)S_{12}(\hat{r}) + V_{\rm LS}(r)\vec{L}\cdot\vec{S} + O(\nabla^2), \tag{2.8}$$

where $S_{12}(\hat{r}) \equiv 3(\vec{\sigma}_1\cdot\hat{r})(\vec{\sigma}_2\cdot\hat{r}) - \vec{\sigma}_1\cdot\vec{\sigma}_2$, $\vec{L} \equiv i\vec{r}\times\vec{\nabla}$ and $\vec{S} \equiv (\vec{\sigma}_1+\vec{\sigma}_2)/2$ denote the tensor operator, the total angular momentum operator and the total spin operators, respectively. We refer to $V_{\rm C}(r) \equiv V_0(r) + V_\sigma(r)\vec{\sigma}_1\cdot\vec{\sigma}_2$ as the central potential, which is a linear combination of the spin-independent central potential $V_0(r)$ and the spin-dependent central potential $V_\sigma(r)$, i.e., $V_{\rm C}(r) = V_0(r) - 3V_\sigma(r)$ for $S=0$, whereas $V_{\rm C}(r) = V_0(r) + V_\sigma(r)$ for $S=1$. $V_{\rm T}(r)$ and $V_{\rm LS}(r)$ denotes the tensor potential and the spin-orbit (LS) potential. $V_{\rm C}(r)$ and $V_{\rm T}(r)$ terms are at the leading order (LO) which do not contain any derivatives, whereas $V_{\rm LS}(r)$ term is at the next to leading order (NLO) which contains a single derivative.

We emphasize that the scattering phase calculated by using $U(\vec{r},\vec{r}')$ does not depend on a particular choice of interpolating field $N(x)$, although the functional form of the potential $U(\vec{r},\vec{r}')$ depends on a particular choice of interpolating field $N(x)$. This is guaranteed as far as $N(x)$ satisfies Eq. (2.3). (An example of unusable ones is the flat wall type interpolating field, which does not satisfy Eq. (2.3).) Those potentials whose functional forms are different but lead to the same scattering phase are called as phase equivalent potentials. They have the same on-shell information, but they have different off-shell information. Good or bad choice of interpolating fields may be determined by the convenience of the resulting potentials in practical use. A bad choice will lead to a bad convergence of the derivative expansion. As a result, the potential becomes highly non-local and inconvenient.

2.2 Construction of the potential

We first consider a method to obtain the nuclear potential $U(\vec{r},\vec{r}')$ directly from the NBS wave functions. It is possible to obtain the nuclear potential $U(\vec{r},\vec{r}')$ by inversely solving the Schrödinger equation by using NBS wave functions as inputs. The NBS wave functions are obtained from the four point nucleon correlator

$$\begin{aligned} C_{NN}(\vec{x}-\vec{y};t) &\equiv \frac{1}{V}\sum_{\vec{x}} \left\langle 0 \left| T\left[N(\vec{x},t)N(\vec{y},t)\cdot\bar{\mathscr{J}}(t=0)\right]\right| 0\right\rangle \\ &= \sum_{\vec{k}} \psi_{\vec{k}}(\vec{x}-\vec{y})\cdot a_{\vec{k}} \exp\left(-2E_{\vec{k}}t\right), \end{aligned} \tag{2.9}$$

where $a_{\vec{k}} \equiv \langle N(+\vec{k})N(-\vec{k})|\bar{\mathscr{J}}(0)|0\rangle$ denotes the overlap factor. $E_{\vec{k}} \equiv \sqrt{m_N^2+\vec{k}^2}$ denotes the relativistic energy of a single nucleon. To be specific, we restrict ourselves to the singlet-spin sector. By adopting the LO truncation of our non-local potential as $U(\vec{r},\vec{r}') \simeq V_{\rm C}(r)$, the central potential can be obtained from a single NBS wave function for the ground state as

$$V_{\rm C}(r) = \frac{\vec{k}^2}{m_N} - \lim_{t\to\infty}\frac{H_0 C_{NN}(\vec{r},t)}{C_{NN}(\vec{r},t)}, \tag{2.10}$$

where $\vec{k}^2/m_N$ corresponds to the energy of the ground state. Here, t should be large enough to achieve the ground state saturation of $C_{NN}(\vec{r},t)$. Otherwise, contamination of excited states affects

the shape of NBS wave functions for the ground state, which leads to uncertainty of resultant potentials. However, large statistical noise prevents us from going to such a large t region for two-baryon system. In addition, when the spatial volume becomes the larger, it gradually becomes the more difficult to achieve the ground state saturation. Note that a typical energy gap between neighboring state shrinks as $\Delta E \sim O(1/L^2)$ as the spatial extension L becomes large.

There is another method to obtain our potential, which makes it possible to avoid the difficulty associated with the ground state saturation [9]. With this method, the potential $U(\vec{r},\vec{r}')$ is obtained directly from the four-point nucleon correlator through the information of time-evolution. To proceed, we derive an equation which describes the time-evolution of the four-point correlator by utilizing a fact that our potential is independent of energy so that all the equal-time NBS wave functions satisfy Eq. (2.4) for the states with $E_{\vec{k}} \leq E_{\rm th} \equiv 2m_N + m_\pi$. To derive it, we consider a normalized four point correlator

$$R(\vec{r},t) \equiv e^{2m_N t} C_{NN}(\vec{r},t). \tag{2.11}$$

We assume that t is moderately large so that elastic contributions ($E < E_{\rm th}$) dominate intermediate states. Parallel to Eq. (2.9), $R(\vec{r},t)$ is decomposed as

$$R(\vec{r},t) = \sum_{\vec{k}} \psi_{\vec{k}}(\vec{r}) \cdot a_{\vec{k}} \exp\left(-t\Delta W(\vec{k})\right), \tag{2.12}$$

where $\Delta W(\vec{k}) \equiv 2E_{\vec{k}} - 2m_N$. By using an identity $\Delta W(\vec{k}) = \frac{\vec{k}^2}{m_N} - \frac{\Delta W(\vec{k})^2}{4m_N}$, the temporal derivative of $R(\vec{r},t)$ is arranged in the following way:

$$\begin{aligned} -\frac{\partial}{\partial t} R(\vec{r},t) &= \sum_{\vec{k}} \left(\frac{\vec{k}^2}{m_N} - \frac{\Delta W(\vec{k})^2}{4m_N} \right) \psi_{\vec{k}}(\vec{r}) \cdot a_{\vec{k}} \exp\left(-t\Delta W(\vec{k})\right) \\ &= \sum_{\vec{k}} \left(H_0 + U - \frac{1}{4m_N} \frac{\partial^2}{\partial t^2} \right) \psi_{\vec{k}}(\vec{r}) \cdot a_{\vec{k}} \exp\left(-t\Delta W(\vec{k})\right), \end{aligned} \tag{2.13}$$

where U denotes the integration operator associated with the interaction kernel $U(\vec{r},\vec{r}')$. To obtain the second line, we used Eq. (2.4) to replace $\vec{k}^2/m_N$ by $H_0 + U$. We finally arrive at the equation which describes the time-evolution of the normalized four-point correlator:

$$\left(\frac{1}{4m_N} \frac{\partial^2}{\partial t^2} - \frac{\partial}{\partial t} - H_0 \right) R(\vec{r},t) = \int d^3r' U(\vec{r},\vec{r}') R(\vec{r}',t). \tag{2.14}$$

It is important to note that this equation is valid even in the presence of excited states, as far as elastic contributions $E < E_{\rm th}$ dominate the intermediate state.

We give an example to calculate a potential by using Eq. (2.14). To be specific, we restrict ourselves to the singlet-spin sector. By adopting the LO truncation of $U(\vec{r},\vec{r}')$, Eq. (2.14) leads us to a new formula

$$V_{\rm C}(r) = -\frac{H_0 R(\vec{r},t)}{R(\vec{r},t)} - \frac{(\partial/\partial t) R(\vec{r},t)}{R(\vec{r},t)} + \frac{1}{4m_N} \frac{(\partial/\partial t)^2 R(\vec{r},t)}{R(\vec{r},t)}. \tag{2.15}$$

Eq. (2.15) can be used to calculate our potential with much smaller t than Eq. (2.10). For Eq. (2.15) to work, t has to be large enough so that the elastic contributions ($E < E_{\rm th}$) can dominates intermediate states of $R(\vec{r},t)$. In contrast, for Eq. (2.10) to work, t has to be much larger so as to achieve the ground state saturation.

We give an explicit example that, with Eq. (2.15), we do not have to rely on the ground state saturation. For this purpose, we introduce a source function with a single real parameter α as

$$f_\alpha(x,y,z) \equiv 1+\alpha\left(\cos(2\pi x/L)+\cos(2\pi y/L)+\cos(2\pi z/L)\right). \tag{2.16}$$

Note that $f_\alpha(x,y,z)$ reduces to the flat wall source for $\alpha=0$. We use α to arrange the mixture of excited state through the overlap factor $a_{\vec{k}}(\alpha)$ as

$$C_{NN}(\vec{r};t) = \sum_{\vec{k}} \psi_{\vec{k}}(\vec{r})\cdot a_{\vec{k}}(\alpha)\cdot \exp\left(-E_{\vec{k}}t\right). \tag{2.17}$$

$C_{NN}(\vec{r},t)$ is shown in Fig. 1(left) for $\alpha = 0, 0.08, 0.16$ at $t=9$. We see that there are deviations.

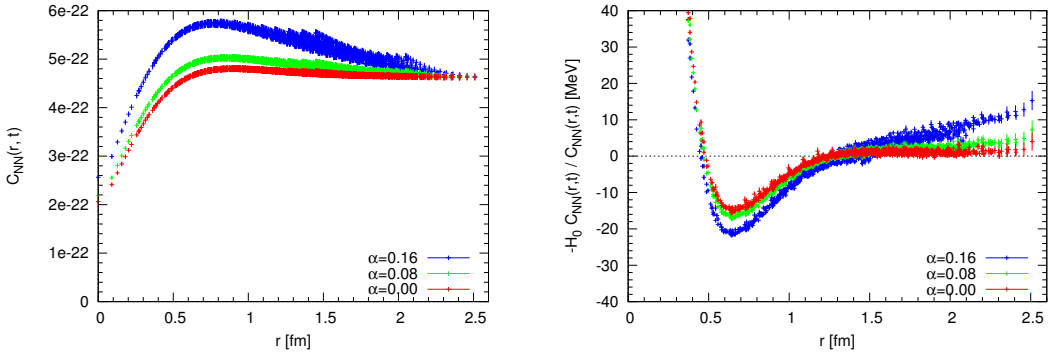

Figure 1: (left) $C_{NN}(\vec{r},t)$ at $t=9$. (right) $-H_0 C_{NN}(\vec{r},t)/C_{NN}(\vec{r},t)$ at $t=9$.

These deviations are due to the different mixture of excited states caused by $a_{\vec{k}}(\alpha)$, which indicates that the contamination of excited states is not negligible at $t=9$ in this example. The contamination is transferred to α dependence of $(H_0 C_{NN}(\vec{r},t))/C_{NN}(\vec{r},t)$, which cannot be absorbed by a single number $\vec{k}^2/m_N$. Fig. 2 (left) shows $V_C(r)$ obtained by the new formula Eq. (2.15). We see that the

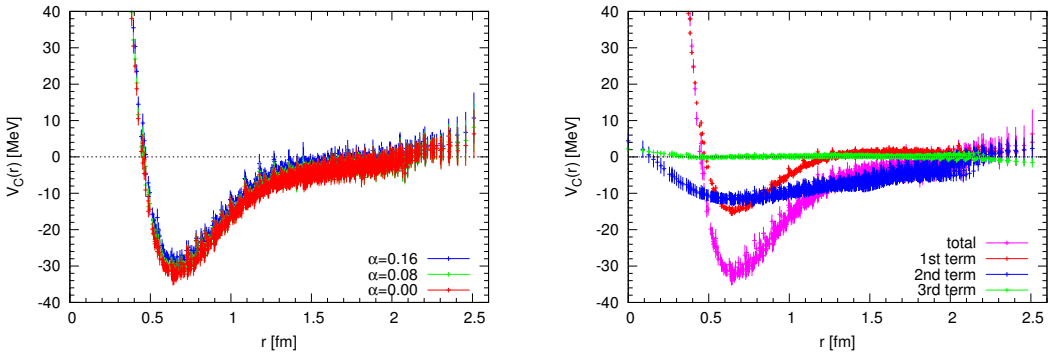

Figure 2: (left) Central potential obtained by the new formula Eq. (2.15). (right) Three contributions to $V_C(r)$ in Eq. (2.15) at $t=9$ for $\alpha=0$.

α dependence disappears within the statistical errors, which indicates that Eq. (2.15) can safely be used in the presence of excited states. Three contributions in Eq. (2.15) are plotted in Fig. 2(right). We see that the first term gives the main trend. The second term gives an important correction. The third term gives a negligible contribution in this example. Note that $\vec{r}$ dependence of the second term can be used as a measure of departure of the ground state saturation, since it has a form of a point-wise effective energy as $-\frac{(\partial/\partial t)R(\vec{r},t)}{R(\vec{r},t)} = -\frac{\partial \log(R(\vec{r},t))}{\partial t}$.

3. Numerical Results

3.1 2+1 flavor QCD results of nuclear forces

By using 2+1 flavor gauge configurations generated by PACS-CS collaboration [26], we present the 2+1 flavor QCD results of nuclear forces $V_{\rm C}(r)$ and $V_{\rm T}(r)$ for the positive parity sector. The gauge configurations are generated by employing the RG improved Iwasaki gauge action at $\beta = 1.9$ with the non-perturbatively $O(a)$ improved Wilson quark action with $C_{\rm SW} = 1.715$ at $\kappa_{ud} = 0.13700, 0.13727, 0.13754$ and $\kappa_s = 0.13640$, which leads to the lattice spacing $a \simeq 0.091$ fm ($a^{-1} = 2.176(31)$ GeV), the spatial extension $L = 32a \simeq 2.90$ fm, the pion mass $m_\pi \simeq 701, 570, 411$ MeV and the nucleon mass $m_N \simeq 1584, 1412, 1215$ MeV, respectively.

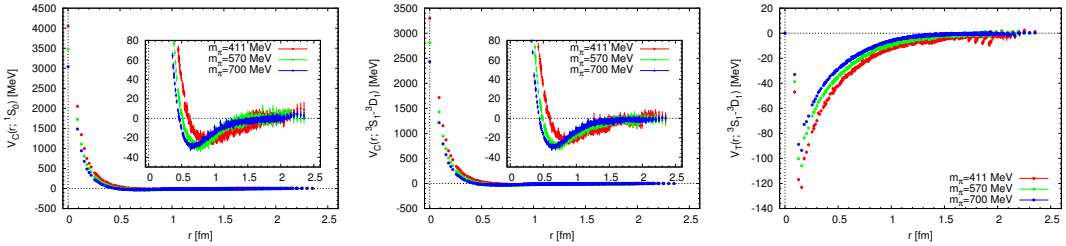

Figure 3: 2+1 flavor QCD result of the spin-singlet central potential, spin-triplet central potential and the tensor potential for the even parity sector for $m_\pi \simeq 411, 570, 701$ MeV.

Fig. 3 shows the 2+1 flavor QCD results of central and tensor potentials for even parity sector. These potentials show the phenomenologically expected properties, i.e., the central potentials have repulsive cores at short distance surrounded by attractive pockets in the medium distance. As the decreasing quark mass, the repulsive core grows, the attractive pockets are enhanced and the strength of tensor potential is enhanced.

We parametrize these potentials by using a functional form of AV18[1]. We perform a simultaneous fit of two $V_{\rm C}(r)$ and one $V_{\rm T}(r)$ by

$$\begin{aligned} V_{C;10}(r) &= -f^2 m_\pi Y_c(r) + I^c_{10} T^2_c(r) + \left(P^c_{10} + (m_\pi r) Q^c_{10} + (m_\pi r)^2 R^c_{10}\right) W_{r_0,a}(r) \\ V_{C;01}(r) &= -f^2 m_\pi Y_c(r) + I^c_{01} T^2_c(r) + \left(P^c_{01} + (m_\pi r) Q^c_{01} + (m_\pi r)^2 R^c_{01}\right) W_{r_0,a}(r) \\ V_{T;01}(r) &= -f^2 m_\pi T_c(r) + I^t_{01} T^2_c(r) + \left(P^t_{01} + (m_\pi r) Q^t_{01} + (m_\pi r)^2 R^t_{01}\right) W_{r_0,a}(r), \end{aligned} \tag{3.1}$$

which have 16 adjustable parameters: $f^2, c, r_0, a, I^c_{10}, P^c_{10}, Q^c_{10}, R^c_{10}, I^c_{01}, P^c_{01}, Q^c_{01}, R^c_{01}, I^t_{01}, P^t_{01}, Q^t_{01}, R^t_{01}$. Suffixes "10" and "01" indicate $T = 1, S = 0$ and $T = 0, S = 1$ respectively. Superindices "c" and "t" indicate "central" and "tensor", respectively. $Y_c(r) \equiv (1 - e^{-cr^2}) e^{-m_\pi r}/(m_\pi r)$ denotes the Yukawa function and $T_c(r) \equiv (1 - e^{-cr^2})^2 (1 + 3/(m_\pi r) + 3/(m_\pi r)^2) e^{-m_\pi r}/(m_\pi r)$ denotes the tensor function with a Gaussian cutoff parameter c at short distance. $W_{r_0,a}(r) \equiv 1/(1 + e^{(r-r_0)/a}$ denotes Woods-Saxon function. Our tensor potential has a cusp at $r = \sqrt{3}a \simeq 0.16$ fm, where a smooth parametrization becomes difficult. To avoid this, we use $r \geq \sqrt{3}a$ as the fitting region for the tensor force, whereas linear interpolation is performed in the region $r < \sqrt{3}a$. As an attempt to take into account a possible artifact of periodic boundary, we use $\bar{V}_{C;190}(\vec{r}) \equiv \sum_{\vec{n} \in \mathbb{Z}^3} V_{c;10}(|\vec{r} - L\vec{n}|)$, $\bar{V}_{C;01}(\vec{r}) \equiv \sum_{\vec{n} \in \mathbb{Z}^3} V_{c;01}(|\vec{r} - L\vec{n}|)$, $\bar{V}_{T;01}(\vec{r}) \equiv \sum_{\vec{n} \in \mathbb{Z}^3} V_{T;01}(|\vec{r} - L\vec{n}|)$, i.e., we use $\bar{V}_{C;10}(\vec{r})$, $\bar{V}_{C;01}(\vec{r})$ and $\bar{V}_{T;01}(\vec{r})$ defined on the finite torus to extract spherically symmetric $V_{C;10}(r)$, $V_{C;01}(r)$ and $V_{T;01}(r)$.

Fig. 4(left) shows the result of the spin-singlet central potential for $m_\pi \simeq 570$ MeV. We see that the lattice data is smoothly parametrized. Deviation of $V_{C;10}(r)$ from $\bar{V}_{C;10}(\vec{r})$ is seen to be less significant, which indicates that $L \simeq 3$ fm is sufficient for $m_\pi \simeq 570$ MeV. (Deviation becomes gradually important at $m_\pi \simeq 411$ MeV.)

These results are used to solve Schrödinger equation for scattering observables. The resultant scattering phase for ${}^1S_0$ channel is shown in Fig. 4(right). We see that the behaviors are qualitatively reasonable. However, the strength is weaker than the experimental one. In addition, they do not tend to approach the experimental one in this quark mass region. Possible reason would be that, in this quark mass region, the repulsive core is enhanced faster than the attractive pocket grows, which indicates the importance of direct lattice QCD calculation at smaller quark mass region. Note that the result indicates that NN interaction is attractive at low energy, but it is not strong enough to make a bound state [2].

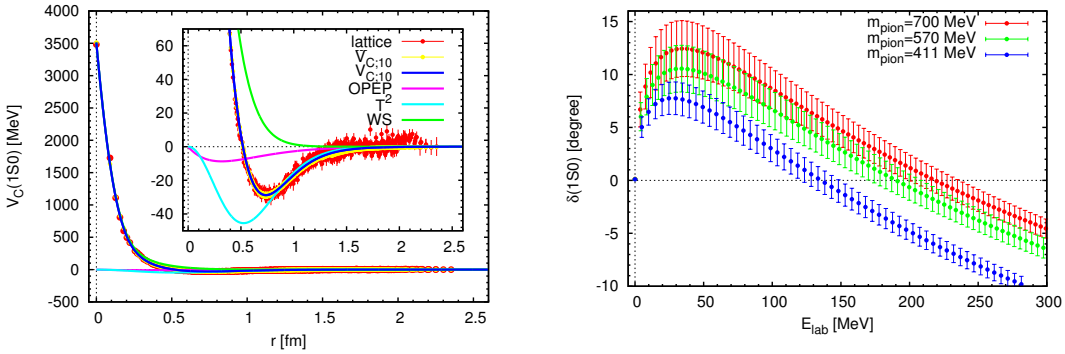

Figure 4: (left) The result of the fit for the spin-singlet central potential for $m_\pi \simeq 570$ MeV. (right) The scattering phase in ${}^1S_0$ channel for $m_\pi \simeq 411, 570, 701$ MeV by using the resultant potentials.

3.2 Nuclear forces for the odd parity sector and the spin-orbit force

Nuclear potentials in odd parity sector have to be determined for complete determination of nuclear potentials on the lattice. These potentials naturally enter the calculation, whenever we study the nuclear matter and multi-nucleon systems involving more than three nucleons. Note that, even if the total multi-nucleon system has even parity, its two-body subsystem can have odd parity.

The spin-orbit potential plays important roles in various phenomena in nuclear physics and astrophysics. It induces the one-body spin-orbit term in the average single-particle nuclear potential, which is used to explain the magic numbers in atomic nuclei. By giving a strong attraction to two nucleon system in ${}^3P_2$ channel at high energy/density, the spin-orbit potential is expected to induce the neutron superfluidity in the neutron stars, which provides a mechanism of neutron star cooling.

As a recent progress, we have extended our method to the nuclear potentials in odd parity sector and the spin-orbit potential [18, 19]. Before, our studies were restricted to the central and the tensor potentials for even parity sector due to a technical reason that "orbital part" of our two-nucleon sources were "s-wave" so that the accessible quantum numbers were restricted to $J^P \simeq 0^+$ and 1^+. To obtain the nuclear potentials for odd parity sectors and the spin-orbit potential, we

[2] This is in conflict with Refs. [27, 28].

employ a momentum wall source, which makes it possible to access the NBS wave functions for $J^P \simeq 0^-, 1^-, 2^-$ with a projection formula based on the cubic group. The central, tensor and spin-orbit potentials in the odd parity sector are obtained by inversely solving coupled Schrödinger equations for ${}^3P_0$, ${}^3P_1$, ${}^3P_2 - {}^3F_2$ channels.

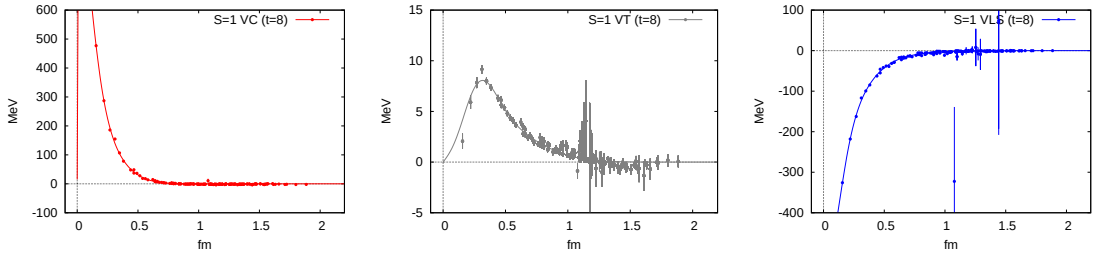

Figure 5: The central (spin-triplet), tensor and spin-orbit potentials for odd parity sector.

The calculation is performed by using 2 flavor gauge configuration generated by CP-PACS collaboration on $16^3 \times 32$ lattice with the RG improved Iwasaki gauge action at $\beta = 1.95$ and $O(a)$ improved Wilson quark action at $\kappa = 0.1375$ and $C_{\rm SW} = 1.53$, which leads to the lattice spacing $a \simeq 0.155$ fm ($a^{-1} = 1.269(14)$ GeV), the spatial extension $L = 16a \simeq 2.49$ fm, the pion mass $m_\pi \simeq 1133$ MeV and the nucleon mass $m_N \simeq 2158$ MeV [29]. Fig. 5 shows the results. We see that the results reproduce qualitative features as (1) $V_{\rm C}(r)$ has a repulsive core. (2) $V_{\rm T}(r)$ is positive and weak. (3) $V_{\rm LS}(r)$ is large and negative.

3.3 Three-nucleon forces

Three-nucleon potential receives a growing interest in nuclear physics and astrophysics. Precision calculations of few-nucleon systems reveal that, although the two-nucleon potential can reproduce a general trend of spectra of few-nucleon system, three-nucleon potential is needed for a quantitative purpose. The three-nucleon potential has a large influence on the supernova explosion and the structure of neutron star, because the three-nucleon potential is expected to play a more important role at high density. However, experimental data is still limited, and the phenomenological construction of three-nucleon potential has to involve inevitable uncertainty.

It is possible to apply our lattice QCD method to construct three-nucleon potential, which however requires enormous calculational resources. Although a calculation of three-nucleon potential at all spatial points does not seem to be realistic for the moment[3], it is possible to perform a calculation on restricted spatial region. By using 2 flavor gauge configuration generated by CP-PACS collaboration (same as Sect.3.2), three-nucleon potential is calculated on the three-particle spatial region $\{(\vec{x}_1, \vec{x}_2, \vec{x}_3) | \vec{x}_3 = (\vec{x}_1 + \vec{x}_2)/2\}$, which is referred to as "linear setup" [16, 21]. Fig. 6 shows the result, where the three-nucleon potential in the triton channel is plotted against $r_2 \equiv |\vec{x}_1 - \vec{x}_2|/2$. An indication of repulsion is observed at short distance, while it is small at long distance due to the suppression of two-pion exchange by the heavy pion.

[3]Situations are being improved. New lattice techniques are being accumulated to study multi-baryon system [30, 31, 32].

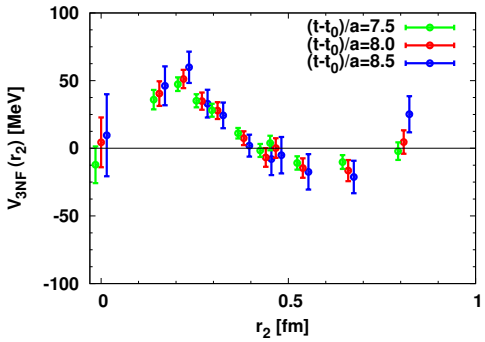

Figure 6: The three-nucleon potential in the triton channel with linear setup.

3.4 Hyperon forces

Hyperon-nucleon (YN) and hyperon-hyperon (YY) interactions serve as important inputs in studying hyper-nuclei and hyperon matter, which is expected to play an important role in neutron star core. However, phenomenological construction of hyperon potentials involves large uncertainty due to the limited experimental information on hyperon scattering data.

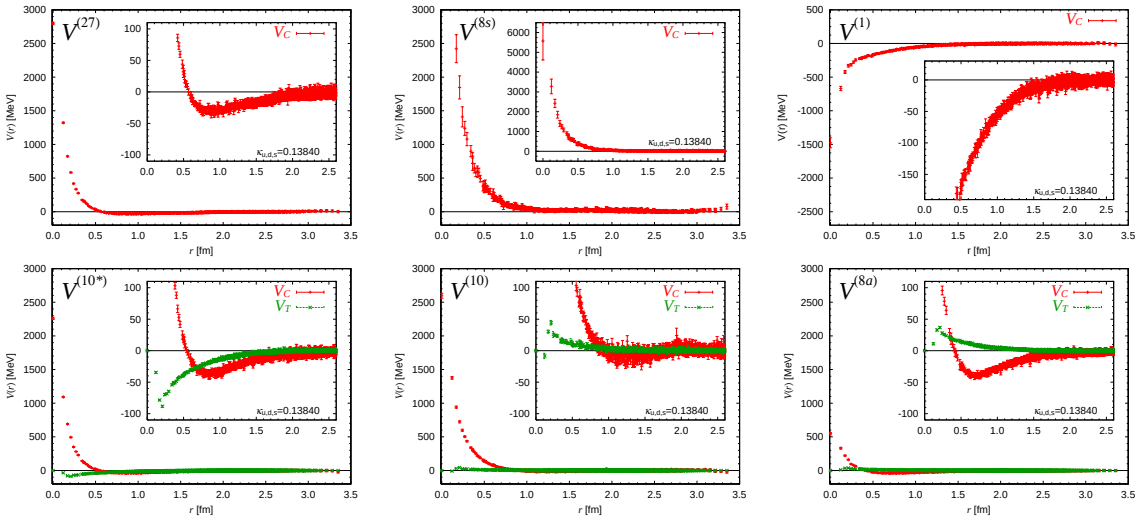

Figure 7: Hyperon potentials in the flavor SU(3) limit.

Hyperon potentials are one of the best targets to apply our lattice QCD method. We have started our calculations from $N\Xi(I=1)$ [12], and then moved to $N\Lambda$ and $N\Sigma(I=3/2)$ [20]. Since there are so many two-hyperon channels, it is better to understand the general trend first by considering the idealized flavor SU(3) limit. In this limit, the flavor structure of two-baryon system is classified by the following six irreducible representations:

$$8 \otimes 8 = \underbrace{27 \oplus 8_S \oplus 1}_{\text{symmetric}} \oplus \underbrace{10^* \oplus 10 \oplus 8_A}_{\text{anti-symmetric}}. \tag{3.2}$$

"symmetric" and "anti-symmetric" refer to the symmetry when flavors of two baryons are exchanged. In even parity sector, tensor potential couples to 10^*, 10 and 8_A, since their total spin S is triplet.

The lattice QCD calculation is performed by using 3 flavor QCD gauge configuration on a $32^3 \times 32$ lattice generated by HAL QCD collaboration by employing the RG improved Iwasaki gauge action at $\beta = 1.83$ and $O(a)$ improved Wilson quark action at $\kappa_{uds} = 0.13840$ with $C_{\rm SW} = 1.761$, which leads to the lattice spacing $a = 0.121(2)$ fm, the spatial extension $L = 32a \simeq 3.87$ fm and hadron masses as $m_{\rm PS} \simeq 469$ MeV, $m_{\rm vec} \simeq 829$ MeV, $m_{\rm baryon} \simeq 1161$ MeV [15].

Fig. 7 shows the central and the tensor potentials in the even parity sector. We see that they show rich flavor structure. Note that two-nucleon system belongs to 27 and 10^*. Therefore, the qualitative behaviors of these two are essentially the same as the conventional nuclear potentials given in Fig. 3. Remarkable difference is found for $V^{(1)}$. It is attractive at all distance involving no repulsive core, and a bound H-dibaryon is found to exist in this channel [14, 15]. Short distance behaviors of these six potentials are consistent with the quark model prediction indicating the importance of quark Pauli blocking effect.

Flavor SU(3) symmetry is broken in the real world. Six irreducible representations begin to couple. Eight octet baryons split into two N, one Λ, three Σ, and two Ξ, and they obtain their own mass, which gives rise to several inelastic thresholds in two-hyperon systems. To study such systems, our method is extended to coupled channel formalism [7], which is first applied to the $\Lambda\Lambda$-$N\Xi$-$\Sigma\Sigma$ coupled system to reveal the nature of H-dibaryon in the real world [22].

4. Summary

We have reported lattice QCD study of baryon-baryon interaction based on the method developed by HAL QCD collaboration. The baryon-baryon potentials are defined from Schrödinger equation by using equal-time Nambu-Bethe-Salpeter (NBS) wave functions. Resultant potentials respect the scattering data, because they are defined to reproduce the scattering phase embedded in the long distance part of the equal-time NBS wave functions. The potentials thus defined can efficiently be calculated from the four-point baryon correlators, which makes it possible to extract the potentials even in the presence of contamination of excited states. These techniques have been applied to many systems. Starting from the central and the tensor NN potentials in even parity sector, it has now been extended to the NN potentials in odd parity sector, the spin-orbit potential, three-nucleon potentials, and various hyperon potentials.

With the growth of the performance of super computers, it will soon become possible to perform these calculations with a realistic setup employing the physical quark mass on a large spatial volume. The results should be applied not only to (hyper) nuclei, but also to astrophysics. Lattice QCD must play a unique role in studying the systems with limited experimental information.

Lattice QCD Monte Carlo calculations have been performed on Blue Gene/L at KEK, T2K at University of Tsukuba and SR16000 at YITP in Kyoto University. We thank CP-PACS and PACS-CS Collaborations [29, 26] and ILDG/JLDG [34] for dynamical QCD gauge configurations. We are grateful for authors and maintainers of CPS++[33], a modified version of which is used in these calculations.

References

[1] V. G. J. Stoks, R. A. M. Klomp, C. P. F. Terheggen and J. J. de Swart, Phys. Rev. C **49** (1994) 2950.

[2] R. B. Wiringa, V. G. J. Stoks and R. Schiavilla, Phys. Rev. C **51** (1995) 38.

[3] R. Machleidt, Phys. Rev. C **63** (2001) 024001

[4] E. Epelbaum, H. -W. Hammer and U. -G. Meissner, Rev. Mod. Phys. **81** (2009) 1773.

[5] N. Ishii, S. Aoki and T. Hatsuda, Phys. Rev. Lett. **99** (2007) 022001.

[6] S. Aoki, T. Hatsuda and N. Ishii, Prog. Theor. Phys. **123** (2010) 89.
S. Aoki, T. Hatsuda and N. Ishii, Comput. Sci. Dis. **1** (2008) 015009.

[7] S. Aoki *et al.* [HAL QCD Collaboration], Proc. Japan Acad. B **87** (2011) 509.

[8] K. Murano, N. Ishii, S. Aoki and T. Hatsuda, Prog. Theor. Phys. **125** (2011) 1225.

[9] N. Ishii *et al.* [HAL QCD Collaboration], Phys. Lett. B **712** (2012) 437.

[10] S.Aoki, B.Charron, T.Doi, T.Hatsuda, T.Inoue, N.Ishii, arXiv:1212.4896 [hep-lat]. Phys.Rev.D in press.

[11] S. Aoki, N. Ishii, T. Doi, Y. Ikeda and T. Inoue, arXiv:1303.2210 [hep-lat].

[12] H. Nemura, N. Ishii, S. Aoki and T. Hatsuda, Phys. Lett. B **673** (2009) 136.

[13] T. Inoue *et al.* [HAL QCD Collaboration], Prog. Theor. Phys. **124** (2010) 591.

[14] T. Inoue *et al.* [HAL QCD Collaboration], Phys. Rev. Lett. **106** (2011) 162002.

[15] T. Inoue *et al.* [HAL QCD Collaboration], Nucl. Phys. A **881** (2012) 28.

[16] T. Doi *et al.* [HAL QCD Collaboration], Prog. Theor. Phys. **127** (2012) 723.

[17] Y. Ikeda [HAL QCD Collaboration], PoS LATTICE **2011** (2011) 159.

[18] K. Murano [HALQCD Collaboration], PoS LATTICE **2011** (2011) 319.

[19] K. Murano *et al.* [HAL QCD Collaboration], in preparation.

[20] H. Nemura [for HAL QCD Collaboration], PoS LATTICE **2011** (2011) 167.

[21] T. Doi [HAL QCD Collaboration], PoS LATTICE **2012** (2012) 009.

[22] K. Sasaki [HAL QCD Collaboration], PoS LATTICE **2012** (2012) 157.

[23] C. J. D. Lin, G. Martinelli, C. T. Sachrajda and M. Testa, Nucl. Phys. B **619** (2001) 467.

[24] S. Aoki *et al.* [CP-PACS Collaboration], Phys. Rev. D **71** (2005) 094504.

[25] M. Luscher, Commun. Math. Phys. **105** (1986) 153; Nucl. Phys. B **354** (1991) 531.

[26] S. Aoki *et al.* [PACS-CS Collaboration], Phys. Rev. D **79** (2009) 034503.

[27] T. Yamazaki, Y. Kuramashi and A. Ukawa, Phys. Rev. D **84** (2011) 054506.
T. Yamazaki, K. -i. Ishikawa, Y. Kuramashi and A. Ukawa, Phys. Rev. D **86** (2012) 074514.

[28] S. R. Beane *et al.* [NPLQCD Collaboration], Phys. Rev. D **85** (2012) 054511.

[29] A.Ali Khan *et al.* [CP-PACS Coll.], Phys.Rev.D**65**(2002)054505 [Erratum-ibid.D**67**(2003)059901].

[30] T. Doi and M. G. Endres, Comput. Phys. Commun. **184** (2013) 117.

[31] W. Detmold and K. Orginos, arXiv:1207.1452 [hep-lat].

[32] J. Gunther, B. C. Toth and L. Varnhorst, arXiv:1301.4895 [hep-lat].

[33] Columbia Physics System (CPS), http://qcdoc.phys.columbia.edu/cps.html

[34] http://www.lqcd.org/ildg; http://www.jldg.org/